Sensors and Materials, Vol. 35, No. 2 (2023) 451–458
MYU Tokyo

S & M 3181

Optical and Scintillation Characteristics of Tb-doped $La_2Si_2O_7$ Single Crystal

Prom Kantuptim,[1*] Takumi Kato,[1] Daisuke Nakauchi,[1]
Noriaki Kawaguchi,[1] Kenichi Watanabe,[2] and Takayuki Yanagida[1]

[1]Division of Materials Science, Graduate School of Science and Technology,
Nara Institute of Science and Technology, 8916-5 Takayama, Ikoma, Nara 630-0192, Japan
[2]Department of Applied Quantum Physics and Nuclear Engineering, Faculty of Engineering, Kyushu University,
744 Motooka, Nishi, Fukuoka 819-0395, Japan

(Received September 30, 2022; accepted January 11, 2023)

Keywords: pyrosilicate, Tb^{3+}, pulse height, ionizing radiation

Lanthanum pyrosilicate $La_2Si_2O_7$ (LaPS) single crystals were successfully fabricated by the floating zone (FZ) method with Tb doping concentrations of 0.1, 0.5, 1.0, and 2.0% for scintillation and photoluminescence (PL) study. X-ray diffraction patterns of the samples indicate a single phase of LaPS from their consistency with the reference pattern. Tb-doped LaPS has multiple emissions from Tb^{3+} 4f–4f transitions including those at 380, 420, 440, 480, 540, 590, and 620 nm, as observed in both PL and X-ray-induced scintillation spectra with a PL quantum yield of up to 50.1%. The PL and scintillation decay time constants obtained were 2.64–3.26 and 1.54–2.00 ms, respectively. In ^{137}Cs (662 keV) γ-ray pulse area spectra, the 1.0% Tb-doped LaPS had the highest scintillation light yield of 47700 ph/MeV. From all the results in this study, the optimum Tb doping concentration in LaPS single crystals is considered to be 1.0% for scintillator application.

1. Introduction

The development of ionizing radiation detection systems is crucial for society. In general, materials with the capability of converting ionizing radiation to UV and visible light, the so-called scintillators, combined with photodetectors are used for radiation detection (scintillation detectors).[1,2] In the academic and industrial sectors, the development of novel high-performance scintillator materials is playing a major role in improving the capability of radiation detection. Examples of fields that utilize scintillation detectors include astrophysics,[3] geophysics,[4] medicine,[5,6] environmental observation,[7] and natural resource exploration.[8,9] In addition, scintillator materials have many forms including glasses,[10–13] translucent ceramics,[14–17] plastics,[18,19] organic–inorganic composites,[20–22] and single crystals.[23–26]

Single-crystal scintillators are a preferred and common form of materials because of their high transparency, high effective atomic number, high light yield, physical durability, and

*Corresponding author: e-mail: prom.kantuptim.pf2@ms.naist.jp
https://doi.org/10.18494/SAM4141

ISSN 0914-4935
https://myukk.org/

chemical stability. Well-known examples are $CdWO_4$[27] and Tl-doped NaI.[28] Recently, an interesting trend in single-crystal scintillator research has been pyrosilicate crystals since the development of Ce-doped $Lu_2Si_2O_7$ with a light yield of 26300 ph/MeV and a decay time of 38 ns.[29] More recently, rare-earth pyrosilicates doped with a lanthanide ion have been intensively investigated, including Pr-doped $Lu_2Si_2O_7$,[30] Ce-doped $Y_2Si_2O_7$,[31] and Pr-doped $Gd_2Si_2O_7$.[32] Previously, it was difficult to investigate the scintillation properties of Tb-doped scintillators due to limitations imposed by the pulse height setup, which resulted in the underestimation of the scintillation light yield of scintillators with a decay time in the ms range. A special pulse area setup has recently been developed for scintillators with ms decay time, using which a light yield of 23000 ph/MeV for Tb-doped $Sr_2Gd_8(SiO_4)_6O_2$ was reported.[33] This study is the combination of the newly discovered pyrosilicate, LaPS single crystals[34,35] with Tb as a luminescence center. This is the first report on the Tb concentration dependence of both the photoluminescence (PL) and scintillation properties of Tb-doped LaPS single crystals. The measurements in this study, including the PL emission, PL decay time, scintillation spectrum, scintillation decay time, and recently introduced pulse area spectrum, are designed to provide the comprehensive properties, trends, and potential of Tb-doped LaPS for scintillator application.

2. Materials and Methods

First, 99.99% purity powder comprising SiO_2, Tb_4O_7, and La_2O_3 is weighted and mixed in an agate mortar. The Tb doping concentrations used are 0.1, 0.5, 1.0, and 2.0 mol% with respect to La. The mixed powder is shaped into rods by applying isostatic pressure. Then, the compressed powder rods are sintered in a furnace for 10 h at 1400 °C. After sintering, single crystals are grown from the ceramic rods in a desktop floating zone (FZ) furnace (FZD0192, Canon Machinery) with a crystal growth rate of 4 mm/h. The obtained single crystal rods are cut to a flat tablet shape of 1 mm thickness and polished on both sides. The crystal pieces remaining after the cutting process are ground for use in powdered X-ray diffraction (XRD; MiniFlex600, Rigaku).

The PL emission contour graph and PL quantum yield (*QY*) are obtained using a Quantaurus-QY system (C11347-01, Hamamatsu Photonics) with excitation wavelengths of 250–400 nm and observation wavelengths of 300–700 nm. On the other hand, the PL decay time is analyzed using a Quantaurus-τ system (C11367, Hamamatsu Photonics). The excitation light is controlled by a halogen lamp with a 265 nm bandpass filter, and the observation wavelength is 550 nm.

X-ray-induced scintillation spectra are obtained using our original setup.[36] The irradiated X-ray dose used for the observation is 1 Gy. The X-ray induced scintillation decay time is also obtained using our original system equipped with a pulsed X-ray source and an afterglow characterization system.[37] The observation wavelength is 160–650 nm. The pulse height spectra and absolute scintillation light yield are measured using the recently developed ms decay time pulse area setup.[33] In this measurement, the pulse area is integrated to the number of channels with a pulse shape similar to the pulse height spectrum in the conventional pulse height setup. ^{137}Cs is used as the γ-ray source (662 keV). In addition, $Bi_4Ge_3O_{12}$ (BGO) with a scintillation light yield of 8200 ph/MeV is used as a reference sample for the light yield calculation.[38]

3. Results and Discussion

3.1 Sample conditions

Figure 1(a) presents a Tb-doped LaPS single-crystal rod with a diameter of 4 mm and a length of 18–23 mm. The notable cracks throughout the length of the sample single-crystal rod are typically observed for the pyrosilicate single crystals grown by the FZ method.[39] After cutting and polishing, the Tb-doped LaPS samples are colorless and transparent for every Tb doping concentration, as shown in Fig. 1(b). However, under 254 nm UV irradiation, the Tb-doped LaPS samples exhibit stable luminescence with colors of violet-blue for the 0.1% Tb-doped sample, blue-green for the 0.5% Tb-doped sample, and bright green for the 1.0 and 2.0% Tb-doped samples, as shown in Fig. 1(c).

Figure 2 shows XRD patterns of the powdered Tb-doped LaPS samples, with the undoped LaPS and JCPDS 82-0729 (LaPS) patterns shown for reference. The consistency between the Tb-doped LaPS samples and the reference XRD patterns indicates a single phase of monoclinic $La_2Si_2O_7$ in the synthesized Tb-doped LaPS samples without the impurity phases found in the phase diagram of the La_2O_3–SiO_2 binary system.[40]

3.2 PL property

Figure 3 presents the PL emission contour graph of each Tb-doped LaPS sample. All the samples have similar emission wavelengths from Tb^{3+} 4f–4f transitions but have different emission intensities. In the violet and blue region (380–450 nm), the 0.1% Tb-doped LaPS sample exhibits a high intensity. However, in the green region (520–600 nm), the 1.0 and 2.0% Tb-doped LaPS samples exhibit a high intensity. For the 0.5% Tb-doped sample, the intensity is similar in both regions. The origin of each emission is discussed later. Regarding the 350–700 nm

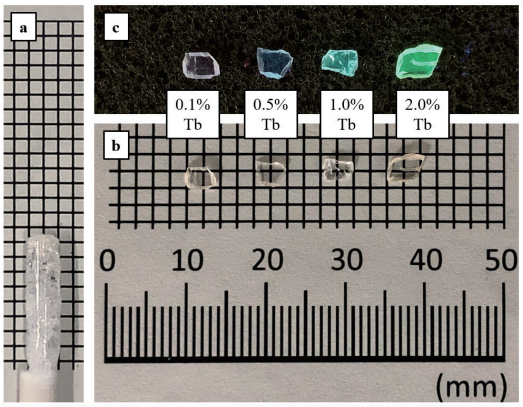

Fig. 1. (Color online) Photographs of Tb-doped LaPS single crystal (a) as-grown, (b) after cutting, and (c) under 254 nm UV irradiation.

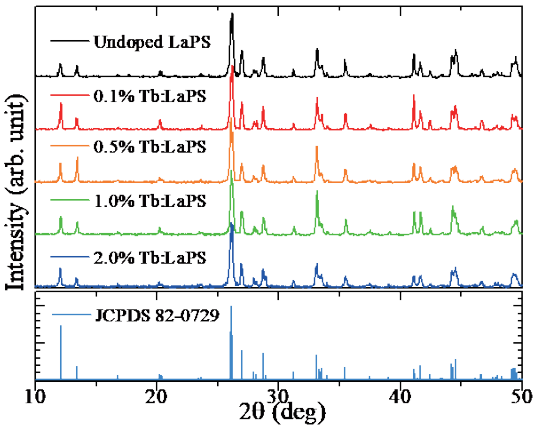

Fig. 2. (Color online) XRD patterns of powdered Tb-doped LaPS samples with undoped LaPS and JCPDS 82-0729 reference patterns.

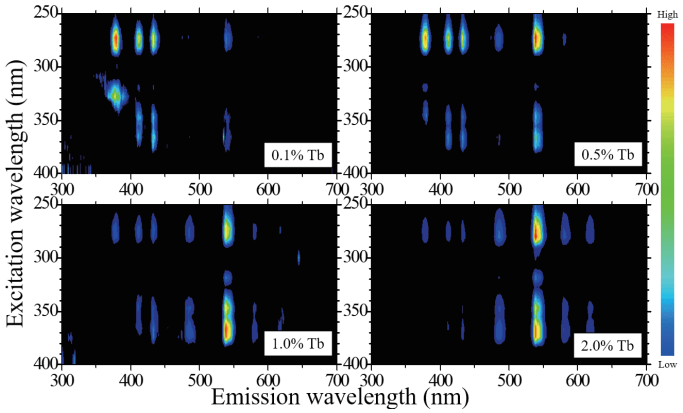

Fig. 3. (Color online) PL emission contour graph of Tb-doped LaPS samples.

emission, the 0.1, 0.5, 1.0, and 2.0% Tb-doped LaPS samples have maximum PL *QY* values of 11.8, 31.7, 26.8, and 50.1%, respectively. In addition, the difference in emission intensity in the color regions and that in PL *QY* in each Tb-doped concentration sample are consistent with the sample appearance (color and brightness) under 254 nm UV light in Fig. 1(c).

Figure 4 presents the PL decay time profiles of the Tb-doped LaPS samples. Each timing profile is fitted by ignoring the instrument response function (IRF) and the slow rise in the initial part of the profile. In another study on Tb-doped scintillators, a slow rise in the PL decay time profile was also observed.[41] The remainder of each profile is fitted with a single exponential function. The decay constant of each sample is also presented in Fig. 4. The 0.5, 1.0, and 2.0% Tb-doped LaPS samples have decay time constants of around 2.64–2.69 ms. On the other hand, the 0.1% Td-doped sample has a PL decay constant of 3.26 ms with a clearly observable slow rise. A possible reason for the slow rise is the inaccuracy of the measurement due to the low-intensity emission of the target sample. However, the fitting is performed without including the slow-rising part, which does not affect the calculation of the decay constant.

3.3 Scintillation property

Figure 5 presents X-ray-induced scintillation spectra of the Tb-doped LaPS samples. All samples have the same spectral shape. Moreover, the scintillation wavelengths of the samples are consistent with the earlier PL emission results. In addition, scintillations from Tb^{3+} 4f–4f transitions including those at 380 mm ($^5D_3 \rightarrow {}^7F_6$), 420 mm ($^5D_3 \rightarrow {}^7F_5$), 440 mm ($^5D_4 \rightarrow {}^7F_5$), 480 mm ($^5D_4 \rightarrow {}^7F_6$), 540 mm ($^5D_4 \rightarrow {}^7F_5$), 590 mm ($^5D_4 \rightarrow {}^7F_4$), and 620 nm ($^5D_4 \rightarrow {}^7F_3$) are found in all samples.[23,42] The intensity on the vertical axis is a qualitative value, and the scintillation light yields are compared using the later pulse area spectral results.

Figure 6 illustrates the X-ray-induced scintillation decay time profiles of the Tb-doped LaPS samples with the fitting functions and decay constants. Each decay time profile is fitted with two exponential decay functions. The first decay constant of all samples is affected by the IRF, which is shown in the initial part of the profile. On the other hand, the second decay constant

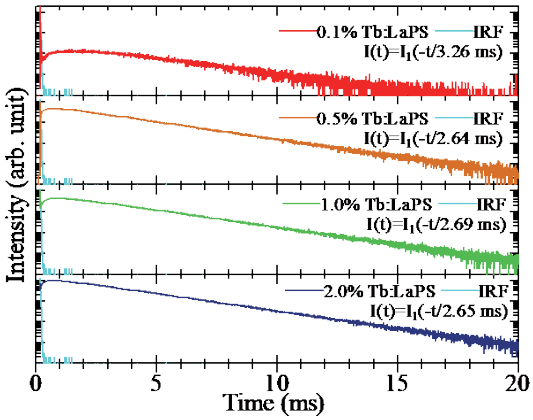

Fig. 4. (Color online) PL decay time profiles of Tb-doped LaPS samples.

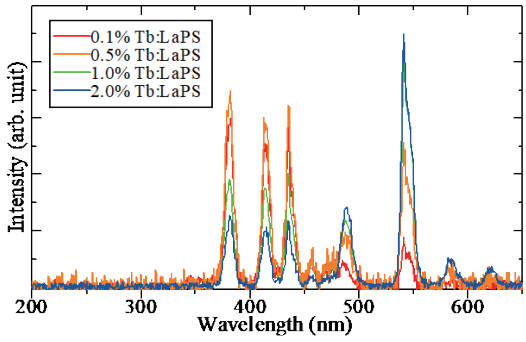

Fig. 5. (Color online) X-ray-induced scintillation spectra of Tb-doped LaPS samples.

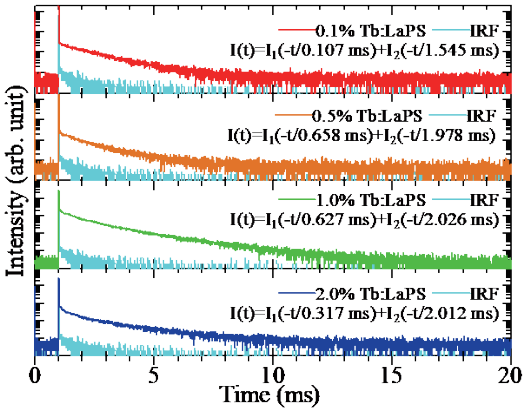

Fig. 6. (Color online) X-ray-induced scintillation decay time profiles of Tb-doped LaPS samples.

originates from scintillations from the Tb^{3+} 4f-4f transitions. Compared with the previous PL decay times, the scintillation decay constants of Tb^{3+} 4f–4f transitions of all samples are small. This trend has also appeared in other studies on the Tb doping concentration dependence.[41,43] This phenomenon may be caused by the emission range of this measurement from 160 to 650 nm, which includes more emissions than the narrower observation wavelength (550 nm) in the PL decay time measurement. In addition, the second decay constants of the 0.5, 1.0, and 2.0% Tb-doped LaPS samples are similar (around 2.00 ms). However, the 0.1% Tb-doped LaPS sample has a decay constant of 1.54 ms. This decrease may be caused by the difficulty in measurement due to the low overall emission intensity of the 0.1% Tb-doped LaPS, as observed in previous results.

Figure 7 presents the ^{137}Cs (662 keV) γ-ray pulse area spectra of the Tb-doped LaPS samples, with the spectrum of BGO as a reference. All samples exhibit a clear photoabsorption peak except for the 0.1% Tb-doped LaPS sample. In the scintillation light yield calculation, the photoabsorption peak channel and the quantum efficiency of the photomultiplier tube (PMT) are

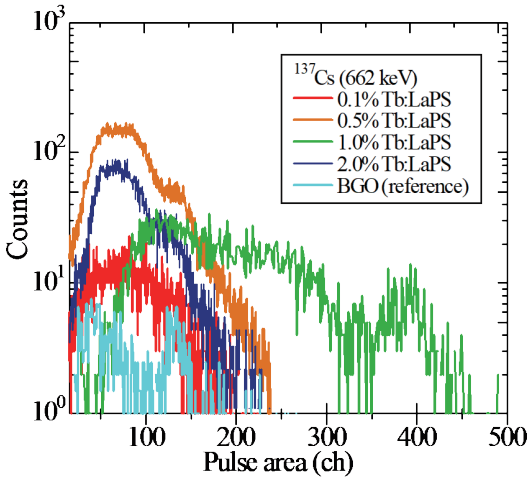

Fig. 7. (Color online) ^{137}Cs pulse area spectra of Tb-doped LaPS samples with BGO as reference.

major considerations. In this PMT (R7600U-200, Hamamatsu Photonics), the BGO reference scintillation wavelength (480 nm) and Tb-doped LaPS sample scintillation wavelength (540 nm) have quantum efficiencies of 25 and 9%, respectively.[33] In the case of the sample and the reference having the same photoabsorption peak channel, the scintillation light yield of the Tb-doped LaPS sample is 2.77 times higher than that of the BGO reference. The 1.0% Tb-doped LaPS sample has the highest scintillation light yield of 47700 ph/MeV, followed by the 0.5, 2.0, and 0.1% Tb-doped LaPS samples with scintillation light yields of 24400, 22400, and 22000 ph/MeV, respectively. This scintillation light yield is higher than those of other oxide scintillators.

4. Conclusions

Single-crystal LaPS samples with Tb doping concentrations of 0.1, 0.5, 1.0, and 2.0 mol% were grown by the FZ method. The XRD results of the samples confirmed the single phase of LaPS. Regarding PL properties, Tb-doped LaPS exhibited multiple emissions from Tb^{3+} 4f-4f transitions with the PL *QY* reaching 50.1% for the 2.0% Tb-doped LaPS sample. PL decay times were 2.64–3.26 ms. Regarding X-ray-induced scintillation properties, Tb-doped LaPS samples exhibited scintillations from Tb^{3+} 4f–4f transitions at multiple wavelengths, similar to the PL emission, with a major scintillation wavelength of 540 nm ($^5D_4 \rightarrow {}^7F_5$). The scintillation decay times of the 0.5, 1.0, and 2.0% LaPS samples were around 2.00 ms, with a scintillation decay time of 1.54 ms for the 0.1% Tb-doped sample. According to ^{137}Cs (662 keV) γ-ray pulse area spectra, the 1.0% Tb-doped LaPS sample had the highest scintillation light yield of 47700 ph/MeV among the Tb-doped LaPS samples. The comprehensive results for the Tb-doped LaPS samples in this work show the possibility of using Tb-doped LaPS as novel scintillators in applications that favor a high light yield over a ms-range decay time such as scintillator screens for radiography.

Acknowledgments

This work is supported by the Cooperative Research Project of the Research Center for Biomedical Engineering, Nippon Sheet Glass Foundation, and Iketani Science and Technology. The Japan Society for the Promotion of Science (JSPS) is acknowledged for Grants-in-Aid for Scientific Research A (22H00309), Scientific Research B (21H03733, 21H03736, and 22H02939), Exploratory Research (22K18997), and Early-Career Scientists (20K20104).

References

1 C. W. E. van Eijk: Nucl. Instrum. Methods Phys. Res. B **460** (2001) 1.
2 T. Yanagida: Proc. Jpn. Acad. Ser. B **94** (2018) 75.
3 M. Kole, M. Chauvin, Y. Fukazawa, K. Fukuda, S. Ishizu, M. Jackson, T. Kamae, N. Kawaguchi, T. Kawano, M. Kiss, E. Moretti, M. Pearce, S. Rydström, H. Takahashi, and T. Yanagida: Nucl. Instrum. Methods Phys. Res. B **770** (2015) 68.
4 A. Parshin, V. Morozov, N. Snegirev, E. Valkova, and F. Shikalenko: Appl. Sci. **11** (2021) 1.
5 C. Ronda, H. Wieczorek, V. Khanin, and P. Rodnyi: ECS J. Solid State Sci. Technol. **5** (2016) R3121.
6 C. L. Melcher: J. Nucl. Med. **41** (2000) 1051.
7 Y. Zou, W. Zhang, C. Li, Y. Liu, and H. Luo: Radiat. Meas. **127** (2019) 106143.
8 T. Yanagida, Y. Fujimoto, S. Kurosawa, K. Kamada, H. Takahashi, Y. Fukazawa, M. Nikl, and V. Chani: Jpn. J. Appl. Phys. **52** (2013) 3.
9 C. L. Melcher: Nucl. Instruments Methods Phys. Res. Sect. B **40**–**41** (1989) 1214.
10 K. Ichiba, Y. Takebuchi, H. Kimura, D. Shiratori, T. Kato, D. Nakauchi, N. Kawaguchi, and T. Yanagida: Sens. Mater. **34** (2022) 677.
11 N. Kiwsakunkran, W. Chaiphaksa, N. Chanthima, H. J. Kim, S. Kothan, A. Prasatkhetragarn, and J. Kaewkhao: Radiat. Phys. Chem. **188** (2021) 109639.
12 D. Shiratori, Y. Takebuchi, T. Kato, D. Nakauchi, N. Kawaguchi, and T. Yanagida: Sens. Mater. **34** (2022) 745.
13 H. Kimura, T. Kato, D. Nakauchi, N. Kawaguchi, and T. Yanagida: Sens. Mater. **34** (2022) 691.
14 H. Kimura, F. Nakamura, T. Kato, D. Nakauchi, G. Okada, N. Kawaguchi, and T. Yanagida: Sens. Mater. **30** (2018) 1555.
15 T. Kato, D. Nakauchi, N. Kawaguchi, and T. Yanagida: Sens. Mater. **32** (2020) 1411.
16 T. Kunikata, T. Kato, D. Shiratori, D. Nakauchi, N. Kawaguchi, and T. Yanagida: Sens. Mater. **34** (2022) 661.
17 D. Shiratori, T. Kato, D. Nakauchi, N. Kawaguchi, and T. Yanagida: Sens. Mater. **33** (2021) 2171.
18 D. Takashima, K. Ozaki, M. Nishimura, N. Okada, D. Akai, and M. Ishida: Sens. Mater. **27** (2015) 1.
19 M. Koshimizu, T. Yanagida, R. Kamishima, Y. Fujimoto, and K. Asai: Sens. Mater. **31** (2019) 1233.
20 A. Horimoto, N. Kawano, D. Nakauchi, H. Kimura, M. Akatsuka, and T. Yanagida: Sens. Mater. **32** (2020) 1395.
21 K. Okazaki, D. Onoda, D. Nakauchi, N. Kawano, H. Fukushima, T. Kato, N. Kawaguchi, and T. Yanagida: Sens. Mater. **34** (2022) 575.
22 M. Koshimizu, N. Kawano, A. Kimura, S. Kurashima, M. Taguchi, Y. Fujimoto, and K. Asai: Sens. Mater. **33** (2021) 2137.
23 D. Nakauchi, T. Kato, N. Kawaguchi, and T. Yanagida: Sens. Mater. **33** (2021) 2203.
24 M. Akatsuka, H. Kimura, D. Onoda, D. Shiratori, D. Nakauchi, T. Kato, N. Kawaguchi, and T. Yanagida: Sens. Mater. **33** (2021) 2243.
25 Y. Fujimoto, D. Nakauchi, T. Yanagida, M. Koshimizu, and K. Asai: Sens. Mater. **34** (2022) 629.
26 H. Fukushima, M. Akatsuka, H. Kimura, D. Onoda, D. Shiratori, D. Nakauchi, T. Kato, N. Kawaguchi, and T. Yanagida: Sens. Mater. **33** (2021) 2235.
27 C. Arnaboldi, J. W. Beeman, O. Cremonesi, L. Gironi, M. Pavan, G. Pessina, S. Pirro, and E. Previtali: Astropart. Phys. **34** (2010) 143.
28 M. Moszyński, J. Zalipska, M. Balcerzyk, M. Kapusta, W. Mengesha, and J. D. Valentine: Nucl. Instrum. Methods Phys. Res., B **484** (2002) 259.
29 L. Pidol, A. Khan-Harari, B. Viana, B. Ferrand, P. Dorenbos, J. T. M. De Haas, C. W. E. van Eijk, and E. Virey: J. Phys. Condens. Matter **15** (2003) 2091.
30 P. Kantuptim, M. Akatsuka, D. Nakauchi, T. Kato, N. Kawaguchi, and T. Yanagida: Radiat. Meas. **134** (2020) 106320.

31 P. Kantuptim, T. Kato, D. Nakauchi, N. Kawaguchi, and T. Yanagida: Radiat. Phys. Chem. **197** (2022) 110160.
32 P. Kantuptim, M. Akatsuka, D. Nakauchi, T. Kato, N. Kawaguchi, and T. Yanagida: Sens. Mater. **32** (2020) 1357.
33 K. Watanabe, T. Yanagida, D. Nakauchi, and N. Kawaguchi: Jpn. J. Appl. Phys. **60** (2021) 106002.
34 Q. Wei, G. Liu, Z. Zhou, J. Wan, H. Yang, and Q. Liu: Mater. Lett. **126** (2014) 178.
35 P. Kantuptim, T. Kato, D. Nakauchi, N. Kawaguchi, and T. Yanagida: Jpn. J. Appl. Phys. **61** (2022) SB1038.
36 T. Yanagida, K. Kamada, Y. Fujimoto, H. Yagi, and T. Yanagitani: Opt. Mater. **35** (2013) 2480.
37 T. Yanagida, Y. Fujimoto, T. Ito, K. Uchiyama, and K. Mori: Appl. Phys. Express **7** (2014) 18.
38 I. Holl, E. Lorenz, and G. Mageras: IEEE Trans. Nucl. Sci. **35** (1988) 105.
39 N. Wolff and D. Klimm: J. Solid State Chem. **312** (2022) 123269.
40 K. Kobayashi and Y. Sakka: J. Ceram. Soc. Japan **122** (2014) 649.
41 N. Kawano, M. Akatsuka, H. Kimura, G. Okada, N. Kawaguchi, and T. Yanagida: Radiat. Meas. **117** (2018) 52.
42 W. Rittisut, N. Wantana, Y. Ruangtaweep, P. Mool-am-kha, S. Rujirawat, P. Manyum, R. Yimnirun, P. Kidkhunthod, A. Prasatkhetragarn, S. Kothan, H. J. Kim, and J. Kaewkhao: Opt. Mater. **121** (2021) 111437.
43 T. Matsuo, T. Kato, H. Kimura, F. Nakamura, D. Nakauchi, N. Kawaguchi, and T. Yanagida: Optik **203** (2020) 163965.